The clustering of galaxies in the SDSS-III Baryon Oscillation Spectroscopic Survey: single-probe measurements from CMASS anisotropic galaxy clustering

Chia-Hsun Chuang,[1,2]★† Francisco Prada,[1,3,4] Marcos Pellejero-Ibanez,[5,6]
Florian Beutler,[7,8] Antonio J. Cuesta,[9] Daniel J. Eisenstein,[10] Stephanie Escoffier,[11]
Shirley Ho,[12] Francisco-Shu Kitaura,[2,7,13] Jean-Paul Kneib,[14,15] Marc Manera,[8,16]
Sebastián E. Nuza,[2] Sergio Rodríguez-Torres,[1,3,17] Ashley Ross,[18]
J. A. Rubiño-Martín,[5,6] Lado Samushia,[8,19,20] David J. Schlegel,[7]
Donald P. Schneider,[21,22] Yuting Wang,[8,23] Benjamin A. Weaver,[24]
Gongbo Zhao,[8,23] Joel R. Brownstein,[25] Kyle S. Dawson,[25]
Claudia Maraston,[8] Matthew D. Olmstead[26] and Daniel Thomas[8]

Affiliations are listed at the end of the paper

ABSTRACT

With the largest spectroscopic galaxy survey volume drawn from the SDSS-III Baryon Oscillation Spectroscopic Survey (BOSS), we can extract cosmological constraints from the measurements of redshift and geometric distortions at quasi-linear scales (e.g. above $50\,h^{-1}$ Mpc). We analyse the broad-range shape of the monopole and quadrupole correlation functions of the BOSS Data Release 12 (DR12) CMASS galaxy sample, at the effective redshift $z = 0.59$, to obtain constraints on the Hubble expansion rate $H(z)$, the angular- diameter distance $D_A(z)$, the normalized growth rate $f(z)\sigma_8(z)$, and the physical matter density $\Omega_m h^2$. We obtain robust measurements by including a polynomial as the model for the systematic errors, and find it works very well against the systematic effects, e.g. ones induced by stars and seeing. We provide accurate measurements $\{D_A(0.59)r_{s,\mathrm{fid}}/r_s, H(0.59)r_s/r_{s,\mathrm{fid}}, f(0.59)\sigma_8(0.59), \Omega_m h^2\} = \{1427 \pm 26\ \mathrm{Mpc}, 97.3 \pm 3.3\ \mathrm{km\,s^{-1}\,Mpc^{-1}}, 0.488 \pm 0.060, 0.135 \pm 0.016\}$, where r_s is the comoving sound horizon at the drag epoch and $r_{s,\mathrm{fid}} = 147.66$ Mpc is the sound scale of the fiducial cosmology used in this study. The parameters which are not well constrained by our galaxy clustering analysis are marginalized over with wide flat priors. Since no priors from other data sets, e.g. cosmic microwave background (CMB), are adopted and no dark energy models are assumed, our results from BOSS CMASS galaxy clustering alone may be combined with other data sets, i.e. CMB, SNe, lensing or other galaxy clustering data to constrain the parameters of a given cosmological model. The uncertainty on the dark energy equation of state parameter, w, from CMB+CMASS is about 8 per cent. The uncertainty on the curvature fraction, Ω_k, is 0.3 per cent. We do not find deviation from flat ΛCDM.

Key words: cosmological parameters – cosmology: observations – distance scale – large-scale structure of Universe.

1 INTRODUCTION

The cosmic large-scale structure from galaxy redshift surveys provides a powerful probe of dark energy and the cosmological model that is highly complementary to the cosmic microwave background (CMB) (e.g. Hinshaw et al. 2013; Planck Collaboration I 2014a), supernovae (SNe) (Riess et al. 1998; Perlmutter et al. 1999), and weak lensing (e.g. see Van Waerbeke & Mellier 2003 for a review).

The scope of galaxy redshift surveys has dramatically increased in the last decade. The 2dF Galaxy Redshift Survey (2dFGRS) obtained 221 414 galaxy redshifts at $z < 0.3$ (Colless et al. 2001,

---

2003), and the Sloan Digital Sky Survey (SDSS; York et al. 2000) collected 930 000 galaxy spectra in the Seventh Data Release (DR7) at $z < 0.5$ (Abazajian et al. 2009). WiggleZ collected spectra of 240 000 emission-line galaxies at $0.5 < z < 1$ over 1000 deg^2 (Drinkwater et al. 2010; Parkinson et al. 2012), and the Baryon Oscillation Spectroscopic Survey (BOSS; Dawson et al. 2013) of the SDSS-III (Eisenstein et al. 2011) is surveying 1.5 million luminous red galaxies (LRGs) at $0.1 < z < 0.7$ over 10 000 deg^2. The newest BOSS data set has been made publicly available in SDSS data release 12 (DR12, Alam et al. 2015, BOSS collaboration). The planned space mission Euclid[1] will survey over 60 million emission-line galaxies at $0.7 < z < 2$ over 15 000 deg^2 (e.g. Laureijs et al. 2011), and the upcoming ground-based experiment DESI[2] (Dark Energy Spectroscopic Instrument) will survey 20 million galaxy redshifts up to $z = 1.7$ and 600 000 quasars ($2.2 < z < 3.5$) over 14 000 deg^2 (Schlegel et al. 2011). The proposed WFIRST[3] satellite would map 17 million galaxies in the redshift range $1.3 < z < 2.7$ over 3400 deg^2, with a larger area possible with an extended mission (Green et al. 2012).

Large-scale structure data from galaxy redshift surveys can be analysed using either the power spectrum or the two-point correlation function. Although these two methods are Fourier transforms of one another, the analysis processes, the statistical uncertainties, and the systematics are quite different and the results cannot be converted using Fourier transform directly because of the finite size of the survey volume. The SDSS-II Luminous Red Galaxy (LRG) (Eisenstein et al. 2001) data have been analysed, and the cosmological results delivered, using both the power spectrum (see, e.g. Tegmark et al. 2004; Hutsi 2005; Blake et al. 2007; Padmanabhan et al. 2007; Percival et al. 2007, 2010; Reid et al. 2010; Montesano, Sanchez & Phleps 2012), and the correlation function method (see, e.g. Eisenstein et al. 2005; Okumura et al. 2008; Cabre & Gaztanaga 2009; Martinez et al. 2009; Sanchez et al. 2009; Kazin et al. 2010; Samushia, Percival & Raccanelli 2011; Chuang, Wang & Hemantha 2012; Padmanabhan et al. 2012; Xu et al. 2013; Hemantha, Wang & Chuang 2014; Oka et al. 2014). Similar analysis have been also applied on the SDSS-III BOSS galaxy sample (Reid et al. 2012, 2014; Tojeiro et al. 2012, 2014; Anderson et al. 2013, 2014a,b; Chuang et al. 2013; Kazin et al. 2013; Manera et al. 2013; Nuza et al. 2013; Samushia et al. 2013, 2014; Sanchez et al. 2013a; Beutler et al. 2014; Wang 2014; Alam et al. 2015; Gil-Marin et al. 2015a,b; Cuesta et al. 2016).

Galaxy clustering allows us to differentiate smooth dark energy and modified gravity as the cause for cosmic acceleration through the simultaneous measurements of the cosmic expansion history $H(z)$ and the growth rate of cosmic large scale structure, $f(z)$ (Guzzo et al. 2008; Wang 2008; Blake et al. 2012). However, to measure $f(z)$, one must determine the galaxy bias b, which requires measuring higher order statistics of the galaxy clustering (see Verde et al. 2001). Song & Percival (2009) proposed using the normalized growth rate, $f(z)\sigma_8(z)$, which would avoid the uncertainties from the galaxy bias. Percival & White (2009) developed a method to measure $f(z)\sigma_8(z)$ and applied it on simulations. Wang (2012) estimated expected statistical constraints on dark energy and modified gravity, including redshift-space distortions and other constraints from galaxy clustering, using a Fisher matrix formalism.

In principle, the Hubble expansion rate $H(z)$, the angular diameter distance $D_A(z)$, the normalized growth rate $f(z)\sigma_8(z)$, and the physical matter density $\Omega_m h^2$ can be well constrained by analysing the galaxy clustering data alone. Eisenstein et al. (2005) demonstrated the feasibility of measuring $\Omega_m h^2$ and an effective distance, $D_V(z)$, from the SDSS DR3 (Abazajian et al. 2005) LRGs, where $D_V(z)$ corresponds to a combination of $H(z)$ and $D_A(z)$. Chuang & Wang (2012) measured $H(z)$ and $D_A(z)$ simultaneously using the galaxy clustering data from the two dimensional two-point correlation function of SDSS DR7 (Abazajian et al. 2009) LRGs. Chuang & Wang (2013a,b) improved the method and modelling to measure $H(z)$, $D_A(z)$, $f(z)\sigma_8(z)$, and $\Omega_m h^2$ from the same data.

Samushia et al. (2011) determined $f(z)\sigma_8(z)$ from the SDSS DR7 LRGs. Blake et al. (2012) measured $H(z)$, $D_A(z)$, and $f(z)\sigma_8(z)$ from the WiggleZ Dark Energy Survey galaxy sample. Reid et al. (2012) and Chuang et al. (2013) measured $H(z)$, $D_A(z)$, and $f(z)\sigma_8(z)$ from the SDSS BOSS DR9 CMASS.

In this study, we apply the similar approach as Chuang & Wang (2013a,b) and Chuang et al. (2013) to determine $H(z)$, $D_A(z)$, and $f(z)\sigma_8(z)$, which extracts a summary of the cosmological information from the large-scale structure of the SDSS BOSS DR12 CMASS alone by using very wide flat priors on the cosmological parameters which are not well constrained by galaxy clustering. We make some modifications from the methodologies used in previous works. First, we extract the cosmological information only using the correlation function at very large scales, i.e. $>55 h^{-1}$ Mpc to minimize the uncertainties from the effect at smaller scales, e.g. non-linear effect, non-linear redshift space distortion, and scale-dependent bias. Note that this strategy can only be applied to the analyses in configuration space since in Fourier space the uncertainties at small scales will propagate to wide k range. We will validate our method using mock catalogues. Secondly, it is known that some observational systematics can distort the observed galaxy clustering at the large scales we are interested in (e.g. Ross et al. 2012). Although we apply the systematics weights to minimize their impact (see Reid et al. 2016), it is not granted that we have removed them completely. In this study, we include a polynomial as the model correcting observational systematic errors, e.g. ones induced by stars and seeing. We will show that our measurements are robust even in the case that we do not use the systematic weight corrections. One can combine our single-probe measurements with other data sets (i.e. CMB, SNe, etc.) to constrain the cosmological parameters of a given dark energy model.

This paper is organized as follows. In Section 2, we introduce the SDSS-III/BOSS DR12 CMASS galaxy sample and mock catalogues used in our study. In Section 3, we describe the details of the methodology that constrains cosmological parameters from our galaxy clustering analysis. In Section 4, we present our single-probe cosmological measurements. In Section 5, given some simple dark energy models, we present the cosmological constraints from our measurements and the combination with other data sets. In Section 6, we compare our measurements with the prediction of *Planck* assuming ΛCDM and other measurements obtained from galaxy clustering data. We summarize and conclude in Section 7.

2 DATA SETS

2.1 The CMASS galaxy catalogues

The Sloan Digital Sky Survey (SDSS; Fukugita et al. 1996; Gunn et al. 1998; York et al. 2000; Smee et al. 2013) mapped over one quarter of the sky using the dedicated 2.5 m Sloan Telescope (Gunn

---

et al. 2006). The Baryon Oscillation Sky Survey (BOSS, Eisenstein et al. 2011; Bolton et al. 2012; Dawson et al. 2013) is part of the SDSS-III survey. It is collecting the spectra and redshifts for 1.5 million galaxies, 160 000 quasars and 100 000 ancillary targets. The Data Release 12 (Alam et al. 2015, BOSS collaboration) has been made publicly available[4]. We use galaxies from the SDSS-III BOSS DR12 CMASS catalogue in the redshift range $0.43 < z < 0.75$. CMASS samples are selected with an approximately constant stellar mass threshold (Eisenstein et al. 2011); We are using 800 853 CMASS galaxies. The effective redshifts of the sample are $z = 0.59$. The details of generating this sample are described in Reid et al. (2016).

2.2 The mock catalogues

For the data release 9, 10, and 11, PTHalos mock catalogues (Manera et al. 2013, 2015) were used for constructing the covariance matrix of the clustering measurements. For the data release 12 (this study), we use 2000 BOSS DR12 MultiDark-PATCHY (MD-PATCHY) mock galaxy catalogues (Kitaura et al. 2016) for validating our methodology and estimating the covariance matrix in this study. These mock catalogues were constructed using a similar procedure described in Rodriguez-Torres et al. 2016 where they constructed the BOSS DR12 lightcone mock catalogues using the MultiDark *N*-body simulations (Klypin et al. 2016). However, instead of using *N*-body simulations, the 2000 MD-PATCHY mocks catalogues were constructed using the PATCHY approximate simulations. These mocks are produced using ten boxes at different redshifts that are created with the PATCHY-code (Kitaura, Yepes & Prada 2014). The PATCHY-code can be composed into two parts: (1) computing approximate dark matter density field; and (2) populating galaxies from dark matter density field with the biasing model. The dark matter density field is estimated using Augmented Lagrangian Perturbation Theory (ALPT; Kitaura & Hess 2013) which combines the second order perturbation theory (2LPT) and spherical collapse approximation. The biasing model includes deterministic bias and stochastic bias (see Kitaura et al. 2014, 2015 for details). The velocity field is constructed based on the displacement field of dark matter particles. The modelling of finger-of-god has also been taken into account statistically. The mocks match the clustering of the galaxy catalogues for each redshift bin (see Kitaura et al. (2016) for details). The mock catalogues were constructed assuming ΛCDM *Planck* cosmology with $\{\Omega_M = 0.307115, \Omega_b = 0.048206, \sigma_8 = 0.8288, n_s = 0.96 \}$, and a Hubble constant ($H_0 = 100\,h\,\mathrm{km\,s^{-1}\,Mpc^{-1}}$) given by $h = 0.6777$. As shown in a mock catalogue comparison study (Chuang et al. 2015), PATCHY mocks are accurate within 5 per cent on scales larger than 5 Mpc h^{-1} (or *k* smaller than 0.5 h Mpc^{-1} in Fourier space) for monopole and within 10–15 per cent for quadrupole. Kitaura et al. (2016) had also demonstrated the accuracy of BOSS PATCHY mock catalogues which are in very good agreement with the observed data in terms of two- and three-point statistics.

3 METHODOLOGY

In this section, we describe the measurement of the multipoles of the correlation function from the observational data, construction of the theoretical prediction, and the likelihood analysis that leads to constraining cosmological parameters and dark energy.

3.1 Measuring the two-dimensional two-point correlation function

We convert the measured redshifts of the BOSS CMASS galaxies to comoving distances by assuming a fiducial model, i.e. flat ΛCDM with $\Omega_m = 0.307115$ and $h = 0.6777$ which is the same model adopted for constructing the mock catalogues (see Kitaura et al. 2016). We use the two-point correlation function estimator given by Landy & Szalay (1993):

$$\xi(s, \mu) = \frac{\mathrm{DD}(s, \mu) - 2\mathrm{DR}(s, \mu) + \mathrm{RR}(s, \mu)}{\mathrm{RR}(s, \mu)}, \quad (1)$$

where *s* is the separation of a pair of objects and μ is the cosine of the angle between the directions between the line of sight (LOS) and the line connecting the pair the objects. DD, DR, and RR represent the normalized data–data, data–random, and random–random pair counts, respectively, for a given distance range. The LOS is defined as the direction from the observer to the centre of a galaxy pair. Our bin size is $\Delta s = 1\ h^{-1}$ Mpc and $\Delta \mu = 0.01$. The Landy and Szalay estimator has minimal variance for a Poisson process. Random data are generated with the same radial and angular selection functions as the real data. One can reduce the shot noise due to random data by increasing the amount of random data. The number of random data we use is about 50 times that of the real data. While calculating the pair counts, we assign to each data point a radial weight of $1/[1 + n(z)\,P_w]$, where $n(z)$ is the radial number density and $P_w = 10^4\ h^{-3}$ Mpc^3 (see Feldman, Kaiser & Peacock 1994). We include the combination of the observational weights assigned for each galaxy by

$$w_{\mathrm{tot},i} = w_{\mathrm{sys},i} * (w_{rf,i} + w_{fc,i} - 1), \quad (2)$$

where $w_{\mathrm{tot},i}$ is the final weight to assign on a galaxy *i*; $w_{\mathrm{sys},i}$ is for removing the correlation between CMASS galaxies and both stellar density and seeing; $w_{rf,i}$ and $w_{fc,i}$ correct for missing objects due to the redshift failure and fibre collision. The details are described in Reid et al. (2016) (see also Ross et al. 2012). Later, we will also test the impact of systematics by removing $w_{\mathrm{sys},i}$ from the analysis.

3.2 Theoretical two-dimensional two-point correlation function

The theoretical model for linear and quasi-linear scales can be constructed by first and higher order perturbation theory. One can compute the model by adding the first order non-linear corrections to the linear theoretical model. There is no other fitting parameter besides the cosmological parameters (which will be introduced later in this paper). The procedure of constructing theoretical model for quasi-linear scales in redshift space is the following. First, we adopt the cold dark matter model and the simplest inflation model (adiabatic initial condition). Thus, we can compute the linear matter power spectra, $P_{\mathrm{lin}}(k)$, by using CAMB (Code for Anisotropies in the Microwave Background; Lewis, Challinor & Lasenby 2000). The linear power spectrum can be decomposed into two parts:

$$P_{\mathrm{lin}}(k) = P_{\mathrm{nw}}(k) + P_{\mathrm{BAO}}^{\mathrm{lin}}(k), \quad (3)$$

where $P_{\mathrm{nw}}(k)$ is the 'no-wiggle' or pure CDM power spectrum calculated using equation 29 from Eisenstein & Hu (1998). $P_{\mathrm{BAO}}^{\mathrm{lin}}(k)$ is the 'wiggled' part defined by equation (3). The non-linear damping effect of the 'wiggled' part, in redshift space, can be well approximated following Eisenstein, Seo & White (2007) by

$$P_{\mathrm{BAO}}^{\mathrm{nl}}(k, \mu_k) = P_{\mathrm{BAO}}^{\mathrm{lin}}(k) \cdot \exp\left(-\frac{k^2}{2k_\star^2}\left[1 + \mu_k^2(2f + f^2)\right]\right), \quad (4)$$

where μ_k is the cosine of the angle between **k** and the LOS, f is the growth rate, and $k_\star$ is computed following Crocce & Scoccimarro (2006) and Matsubara (2008) by

$$k_\star = \left[\frac{1}{3\pi^2} \int P_{\text{lin}}(k) \mathrm{d}k \right]^{-1/2}. \tag{5}$$

The dewiggled power spectrum is

$$P_{\text{dw}}(k, \mu_k) = P_{\text{nw}}(k) + P_{\text{BAO}}^{\text{nl}}(k, \mu_k). \tag{6}$$

Besides the non-linear redshift distortion introduced above, we include the linear redshift distortion as follows in order to obtain the galaxy power spectrum in redshift space at large scales (Kaiser 1987),

$$P_g^s(k, \mu_k) = b^2 \left(1 + \beta \mu_k^2 \right)^2 P_{\text{dw}}(k, \mu_k), \tag{7}$$

where b is the linear galaxy bias and β is the linear redshift distortion parameter.

We compute the theoretical two-point correlation function, $\xi_{th}(\sigma, \pi)$, for quasi-linear scales by Fourier transforming the non-linear power spectrum $P_g^s(k, \mu_k)$. This task is efficiently performed by using Legendre polynomial expansions and one-dimensional integral convolutions as introduced in Chuang & Wang (2013b). Power spectrum analysis is more sensitive to the non-linear effects than the correlation function analysis since the uncertainty at small scales would propagate to wider range of k. To have some idea, one can compare fig. 4 and fig. 7 in Chuang et al. (2015) and will find that different mock catalogues have similar performance in configuration space but are very different in k-space. As shown in the Eisenstein et al. (2007), the damping of BAO is the major correction of the non-linear effects in the configuration space at the scales interested, e.g. $s > 55 \ h^{-1}$ Mpc. In fig. 7 of Samushia et al. (2014), they showed that the growth rate measured using linear redshift distortion model could be biased by 3 per cent when using the scales larger than $55 \ h^{-1}$ Mpc. The accuracy is acceptable since the uncertainty of our $f(z)\sigma_8(z)$ measurement is about 12 per cent.

3.3 Measure multipoles of the two-point correlation function

The traditional multipoles of the two-point correlation function, in redshift space, are defined by

$$\xi_l(s) \equiv \frac{2l+1}{2} \int_{-1}^{1} \mathrm{d}\mu \, \xi(s, \mu) P_l(\mu), \tag{8}$$

where $P_l(\mu)$ is the Legendre Polynomial ($l = 0$ and 2 here). We integrate over a spherical shell with radius s, while actual measurements of $\xi(s, \mu)$ are done in discrete bins. To compare the measured $\xi(s, \mu)$ and our theoretical model, the last integral in equation (8) should be converted into a sum,

$$\hat{\xi}_l(s) \equiv \frac{\displaystyle\sum_{s-\frac{\Delta s}{2} < s' < s+\frac{\Delta s}{2}} \sum_{0 \le \mu \le 1} (2l+1)\xi(s', \mu)P_l(\mu)}{\text{Number of bins used in the numerator}}, \tag{9}$$

where $\Delta s = 5 \ h^{-1}$ Mpc in this work.

We are using the scale range $s = 55$–$200 \ h^{-1}$ Mpc and the bin size is $5 \ h^{-1}$ Mpc. The data points from the multipoles in the scale range considered are combined to form a vector, X, i.e.

$$X = \left\{ \hat{\xi}_0^{(1)}, \hat{\xi}_0^{(2)}, ..., \hat{\xi}_0^{(N)}; \hat{\xi}_2^{(1)}, \hat{\xi}_2^{(2)}, ..., \hat{\xi}_2^{(N)}; ... \right\}, \tag{10}$$

where N is the number of data points in each measured multipole; here $N = 29$. The length of the data vector X depends on the number of multipoles used.

3.4 Model for systematic errors

It is well known that the observations could be contaminated by systematic effects. To obtain the robust and conservative measurements, we include a model for systematics. The model is a simple polynomial given by

$$A(s) = a_0 + \frac{a_1}{s} + \frac{a_2}{s^2}. \tag{11}$$

Since the quadrupole is insensitive to the systematics effects of which we are aware (see Fig. 1] or more details in Ross et al. 2012), we include the systematics model for only the monopole of the theoretical model by

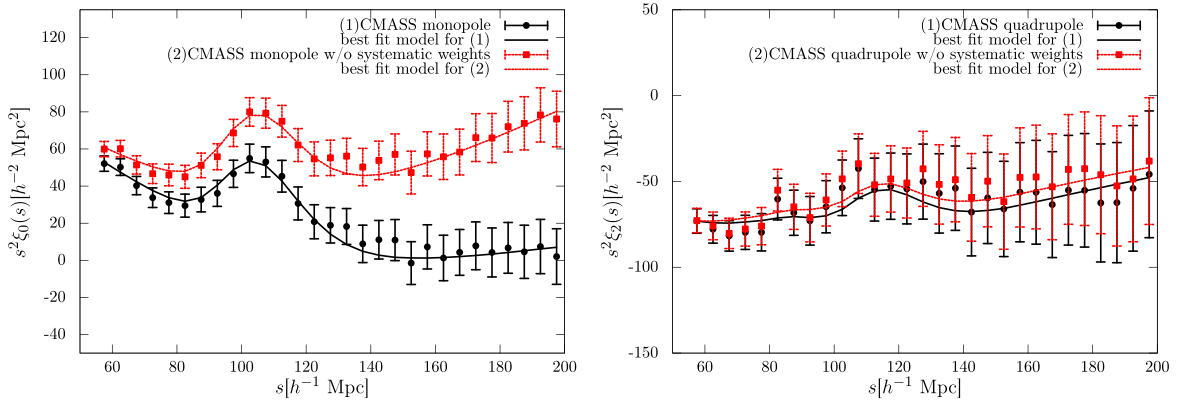$$\xi'_{0,\text{th}}(s) = \xi_{0,\text{th}}(s) + A(s), \tag{12}$$

Figure 1. Measurement of effective monopole (left) and quadrupole (right) of the correlation function from the BOSS DR12 CMASS galaxy sample with/without systematics weights for star and seeing (black/red points), compared to the theoretical models given the parameters measured (solid lines). The error bars are the square roots of the diagonal elements of the covariance matrix. In this study, our fitting scale ranges are $55 \ h^{-1}$ Mpc $< s < 200 \ h^{-1}$ Mpc; the bin size is $5 \ h^{-1}$ Mpc. The minimum χ^2 per degree of freedom is 0.95 for the correlation function computed including the systematics weights; the one without including the systematics weights is 1.05.

where $\xi_{0,\text{th}}(s)$ is the monopole derived from $\xi_{\text{th}}(\sigma, \pi)$ in Section 3.2. Note that $A(s)$ is in the same form as the smooth function used in the BAO-only analyses (e.g. see Xu et al. 2013; Anderson et al. 2014b). In those analyses, two smooth functions have been applied to remove the full shape information of monopole and quadrupole, respectively. However, if we added the smooth function to quadrupole, we would not be able to measure $f(z)\sigma_8(z)$. Fortunately, the quadrupole is insensitive to the systematics as shown in Fig. 1, so that we do not remove its full shape information and thus we can measure $f(z)\sigma_8(z)$.

3.5 Covariance matrix

We use the 2000 mock catalogues created by Kitaura et al. 2016 for the BOSS DR12 CMASS galaxy sample to estimate the covariance matrix of the observed correlation function. We calculate the multipoles of the correlation functions of the mock catalogues and construct the covariance matrix as

$$C_{ij} = \frac{1}{(N-1)(1-D)} \sum_{k=1}^{N} \left(\bar{X}_i - X_i^k \right) \left(\bar{X}_j - X_j^k \right), \qquad (13)$$

where

$$D = \frac{N_b + 1}{N - 1}, \qquad (14)$$

N is the number of the mock catalogues, N_b is the number of data bins, $\bar{X}_m$ is the mean of the mth element of the vector from the mock catalogue multipoles, and X_m^k is the value in the mth elements of the vector from the kth mock catalogue multipoles. The data vector X is defined by equation (10). We also include the correction, D, introduced by Hartlap, Simon & Schneider (2007).

3.6 Likelihood

The likelihood is taken to be proportional to $\exp(-\chi^2/2)$ (Press et al. 1992), with χ^2 given by

$$\chi^2 \equiv \sum_{i,j=1}^{N_X} [X_{\text{th},i} - X_{\text{obs},i}] C_{ij}^{-1} [X_{\text{th},j} - X_{\text{obs},j}] \qquad (15)$$

where N_X is the length of the vector used, X_{th} is the vector from the theoretical model, and X_{obs} is the vector from the observed data.

As explained in Chuang & Wang (2012), instead of recalculating the observed correlation function while computing for different models, we rescale the theoretical correlation function to avoid rendering the χ^2 values arbitrary. This approach can be considered as an application of Alcock-Paczynski effect (Alcock & Paczynski 1979). The rescaled theoretical correlation function is computed by

$$T^{-1}(\xi_{\text{th}}(\sigma, \pi)) = \xi_{\text{th}}\left(\frac{D_A(z)}{D_A^{\text{fid}}(z)}\sigma, \frac{H^{\text{fid}}(z)}{H(z)}\pi \right), \qquad (16)$$

where ξ_{th} is defined in Section 3.2 and χ^2 can be rewritten as

$$\chi^2 \equiv \sum_{i,j=1}^{N_X} \{T^{-1}X_{\text{th},i} - X_{\text{obs},i}^{\text{fid}}\} C_{\text{fid},ij}^{-1} \cdot \{T^{-1}X_{\text{th},j} - X_{\text{obs},j}^{\text{fid}}\}; \qquad (17)$$

where $T^{-1}X_{\text{th}}$ is the vector computed by equation (9) from the rescaled theoretical correlation function, equation (16), taking into account the modelling of observational systematics, equation (11). $X_{\text{obs}}^{\text{fid}}$ is the vector from observed data measured with the fiducial model (see Chuang & Wang 2012 for more details regarding the rescaling method).

3.7 Markov Chain Monte Carlo likelihood analysis

We perform Markov Chain Monte Carlo likelihood analyses using CosmoMC (Lewis & Bridle 2002). The parameter space that we explore spans the parameter set of $\{H(z), D_A(z), \Omega_m h^2, \beta(z), b\sigma_8(z), \Omega_b h^2, n_s, f(z), a_0, a_1, a_2\}$. The quantities Ω_m and Ω_b are the matter and baryon density fractions, n_s is the power-law index of the primordial matter power spectrum, h is the dimensionless Hubble constant ($H_0 = 100h$ km s^{-1} Mpc^{-1}), and $\sigma_8(z)$ is the normalization of the power spectrum. The linear redshift distortion parameter can be expressed as $\beta(z) = f(z)/b$. Thus, one can derive $f(z)\sigma_8(z)$ from the measured $\beta(z)$ and $b\sigma_8(z)$. Among these parameters, only $\{H(z), D_A(z), \Omega_m h^2, \beta(z), b\sigma_8(z)\}$ are well constrained using the BOSS galaxy sample alone in the scale range of interest. We marginalize over the other parameters, $\{\Omega_b h^2, n_s, f(0.59), a_0, a_1, a_2\}$, with the flat priors $\{(0.018\,768, 0.025\,368), (0.8684, 1.0564), (0.3, 1), (-0.003, 0.003), (-3, 3), (-20, 20)\}$, where the flat priors of $\Omega_b h^2$ and n_s are centred on the *Planck* measurements with a width of $\pm 10\sigma_{\text{Planck}}$ (σ_{Planck} is taken from Planck Collaboration XVI 2014b). These priors are sufficiently wide to ensure that CMB constraints are not double counted when our results are combined with CMB data (Chuang et al. 2012).

On the scales we use for comparison with the BOSS galaxy data, the theoretical correlation function only depends on cosmic curvature and dark energy through the parameters $H(z), D_A(z), \beta(z)$, and $b\sigma_8(z)$ assuming that dark energy perturbations are unimportant (valid in the simplest dark energy models). Thus we are able to extract constraints from clustering data that are independent of dark energy.

4 RESULTS

Fig. 1 shows the effective monopole ($\hat{\xi}_0$) and quadrupole ($\hat{\xi}_2$) measured from the BOSS CMASS galaxy sample compared with the theoretical models given the parameters measured. For the CMASS sample, we also present the correlation function measured from the sample without including systematics weights for stars and seeing. We do not test with the systematics weights for fibre collisions and redshift failures because those only affect smallest scales (i.e. $s < 20 \, h^{-1}$ Mpc, see Ross et al. 2012). We will show that the measurements from our methodology are robust against these systematics. The minimum χ^2 per degree of freedom is 0.95 for the correlation function computed including the systematics weights; the one without including the systematics weights is 1.05.

4.1 Measurements of cosmological parameters

With the increasing volume of the galaxy survey, one can obtain the cosmological constraints using the scales which can be modelled simply by perturbation theory (see Section 3.2). We now present the dark energy model independent measurements of the parameters $\{H(0.59), D_A(0.59), \Omega_m h^2, \beta(0.59), \text{and } b\sigma_8(0.59)\}$, obtained by using the method described in previous sections. We also present the derived parameters including $H^{-1}(0.59)r_s/r_{s,\text{fid}}$, $D_A(0.59)r_{s,\text{fid}}/r_s$, and $D_V(0.59)r_{s,\text{fid}}/r_s$ with

$$D_V(z) \equiv \left[(1+z)^2 D_A(z)^2 \frac{cz}{H(z)} \right]^{\frac{1}{3}}, \qquad (18)$$

where r_s is the comoving sound horizon at the drag epoch calculated using equation (6) by CAMB and $r_{s,\text{fid}} = 147.66$ Mpc is the r_s of the fiducial cosmology used in this study (same as the one used by the mock catalogues). $D_V(z)$ is the effective distance which can be

Table 1. Test using the mean of the correlation functions from the mock catalogues. We restore the input values within 0.4σ. The units of H are km s^{-1} Mpc^{-1}, the units of D_A and D_V are Mpc, and ω_m is defined as $\Omega_m h^2$.

	Mean of mocks	Input values	Deviation
$D_A(0.59)r_{s,\text{fid}}/r_s$	1417 ± 28	1409.26	0.29σ
$H(0.59)r_s/r_{s,\text{fid}}$	94.4 ± 3.6	94.09	0.09σ
$f\sigma_8(0.59)$	0.502 ± 0.061	0.4786	0.38σ
$\Omega_m h^2$	0.144 ± 0.016	0.14105	0.20σ
$D_V(0.59)r_{s,\text{fid}}/r_s$	2120 ± 31	2113.37	0.20σ

Table 2. The fiducial measurement and systematic test from the correlation function of DR12 CMASS sample. The systematics test is using the observed correlation function without including the systematics weights (i.e. star and seeing). One can see the measured quantities are robust against these systematics. The units of H are km s^{-1} Mpc^{-1}, the units of D_A and D_V are Mpc.

	Fiducial results	No sys. weights	Difference
$D_A(0.59)r_{s,\text{fid}}/r_s$	1427 ± 26	1422 ± 27	0.18σ
$H(0.59)r_s/r_{s,\text{fid}}$	97.3 ± 3.3	96.7 ± 3.4	0.19σ
$f\sigma_8(0.59)$	0.488 ± 0.060	0.479 ± 0.060	0.15σ
$\Omega_m h^2$	0.135 ± 0.016	0.137 ± 0.016	0.12σ
$D_V(0.59)r_{s,\text{fid}}/r_s$	2107 ± 27	2107 ± 28	0.01σ

measured from the spherical averaged correlation function or power spectrum (e.g. see Eisenstein et al. 2005).

While $H(z)r_s/r_{s,\text{fid}}$ and $D_A(z)r_{s,\text{fid}}/r_s$ measurements are mainly determined by the BAO feature, $\Omega_m h^2$ is basically determined by the overall shape. In Table 3, one can see that the correlations between $\Omega_m h^2$ and both $H(z)r_s/r_{s,\text{fid}}$ and $D_A(z)r_{s,\text{fid}}/r_s$ are small. Since the measurement of monopole is sensitive to the systematics (see Fig. 1), the measurement of $\Omega_m h^2$ would be also sensitive to the systematics and the constraint is weak. However, we still include $\Omega_m h^2$ while using our results to take into account the correlations between $f(z)\sigma_8(z)$ and $\Omega_m h^2$.

Table 1 present our test using the mock catalogues. We apply our methodology on the mean of 2000 correlation functions from the mock catalogues and restore their input values within 0.4σ which shows that one can obtain reasonable results even with such simple model we are using. Note that the simplicity/speed of the model is critical for this work since we are scanning very large parameter space (with wide flat priors) and including the nuisance parameters for modelling the observational systematics. We will investigate more accurate models in the future work (Chuang et al. 2016).

Table 2 lists the mean, rms variance, and 68 per cent confidence level limits for $H^{-1}(0.59)r_s/r_{s,\text{fid}}$, $D_A(0.59)r_{s,\text{fid}}/r_s$, $f(0.59)\sigma_8(0.59)$, $\Omega_m h^2$, and $D_V(0.59)r_{s,\text{fid}}/r_s$} derived in an MCMC likelihood anal-

ysis from the measured $\hat{\xi}_0 + \hat{\xi}_2$ of the DR12 CMASS correlation function.

Table 3 presents the normalized covariance matrix for this parameter set measured using $\hat{\xi}_0 + \hat{\xi}_2$. The correlation between $\Omega_m h^2$ and $H^{-1}(0.59)r_s/r_{s,\text{fid}}$ or $D_A(0.59)r_{s,\text{fid}}/r_s$ are close to zero. However, the correlation coefficient of $f(0.59)\sigma_8(0.59)$ and $\Omega_m h^2$ is about -0.5. Therefore, we include $\Omega_m h^2$ to our product while the constraint of $\Omega_m h^2$ is weak comparing to the one from CMB.

4.2 Using our results from galaxy clustering only

In this section, we describe the steps to combine our results with other data sets assuming some dark energy models. Here, we use the results from CMASS quasi-linear scales as an example. For a given model and cosmological parameters, one can compute $H^{-1}(0.59)r_s/r_{s,\text{fid}}$, $D_A(0.59)r_{s,\text{fid}}/r_s$, $f(0.59)\sigma_8(0.59)$, $\Omega_m h^2$. From Tables 2 and 3, one can derive the covariance matrix, M_{ij}, of these three parameters. Then, χ^2 can be computed by

$$\chi^2 = \Delta_{\text{CMASS}} M_{ij}^{-1} \Delta_{\text{CMASS}}, \tag{19}$$

where

$$\Delta_{\text{CMASS}} = \begin{pmatrix} D_A(0.59)r_{s,\text{fid}}/r_s - 1427 \\ H(0.59)r_s/r_{s,\text{fid}} - 97.3 \\ f(0.59)\sigma_8(0.59) - 0.488 \\ \Omega_m h^2 - 0.135 \end{pmatrix} \tag{20}$$

and

$$M_{ij} = \begin{pmatrix} 6.77E+02 & 3.58E+01 & 4.36E-01 & 5.24E-02 \\ 3.58E+01 & 1.11E+01 & 5.77E-02 & 2.88E-03 \\ 4.36E-01 & 5.77E-02 & 3.57E-03 & -4.62E-04 \\ 5.24E-02 & 2.88E-03 & -4.62E-04 & 2.53E-04 \end{pmatrix}, \tag{21}$$

where M_{ij} can be derived from Tables 2 and 3. Note Table 3 shows the normalized covariance matrix N_{ij}, and M_{ij} can be derived by $M_{ij} = N_{ij}\sigma_i\sigma_j$, where σ_i or σ_j are the standard deviations of the fiducial results in Table 2.

5 ASSUMING DARK ENERGY MODELS

In this section, we present examples of combining our CMASS clustering results with the *Planck* CMB data (Planck Collaboration I 2015) assuming specific dark energy models.

Table 4 shows the cosmological constraints assuming ΛCDM, oΛCDM (non-flat ΛCDM), wCDM (constant equation of state of dark energy), owCDM, $w_0 w_a$CDM, and o$w_0 w_a$CDM. Table 5 shows the cosmological constraints obtained from the correlation function without observational systematics corrections. We find it agrees very well with Table 4. We also present the 2D marginalized

Table 3. Normalized covariance matrix of the fiducial measurements from CMASS galaxy sample (using $55 < s < 200 \ h^{-1}$ Mpc). The units of H are km s^{-1} Mpc^{-1}, the units of D_A and D_V are Mpc.

	$\dfrac{D_A(0.59)}{r_s/r_{s,\text{fid}}}$	$\dfrac{H(0.59)}{r_{s,\text{fid}}/r_s}$	$f\sigma_8(0.59)$	$\Omega_m h^2$	$\dfrac{D_V(0.59)}{r_s/r_{s,\text{fid}}}$
$D_A(0.59)r_{s,\text{fid}}/r_s$	1.0000	0.4129	0.2806	0.1266	0.5849
$H(0.59)r_s/r_{s,\text{fid}}$	0.4129	1.0000	0.2897	0.0543	-0.4969
$f\sigma_8(0.59)$	0.2806	0.2897	1.0000	-0.4856	0.0091
$\Omega_m h^2$	0.1266	0.0543	-0.4856	1.0000	0.0742
$D_V(0.59)r_{s,\text{fid}}/r_s$	0.5849	-0.4969	0.0091	0.0742	1.0000

Table 4. The cosmological constraints from our CMASS measurements combining with *Planck* data assuming ΛCDM, non-flat ΛCDM (oΛCDM), wCDM, owCDM, w_0w_aCDM and ow_0w_aCDM. The units of H_0 are $\mathrm{km\,s^{-1}\,Mpc^{-1}}$.

	Ω_m	H_0	σ_8	Ω_k	w or w_0	w_a
ΛCDM	0.308 ± 0.010	67.8 ± 0.7	0.815 ± 0.009	0	-1	0
oΛCDM	0.311 ± 0.011	67.4 ± 1.1	0.812 ± 0.010	-0.001 ± 0.003	-1	0
wCDM	0.314 ± 0.021	67.2 ± 2.3	0.810 ± 0.022	0	-0.98 ± 0.08	0
owCDM	0.313 ± 0.024	67.3 ± 2.4	0.810 ± 0.024	-0.001 ± 0.004	-0.99 ± 0.11	0
w_0w_aCDM	0.332 ± 0.032	65.5 ± 3.2	0.796 ± 0.028	0	-0.76 ± 0.28	-0.63 ± 0.73
ow_0w_aCDM	0.333 ± 0.032	65.3 ± 3.1	0.796 ± 0.028	-0.003 ± 0.004	-0.74 ± 0.27	-0.80 ± 0.74

Table 5. The cosmological constraints from our CMASS measurements without including observation systematics weight corrections combining with *Planck* data assuming ΛCDM, nonflat ΛCDM (oΛCDM), wCDM, owCDM, w_0w_aCDM and ow_0w_aCDM. The units of H_0 are $\mathrm{km\,s^{-1}\,Mpc^{-1}}$.

	Ω_m	H_0	σ_8	Ω_k	w or w_0	w_a
ΛCDM	0.308 ± 0.010	67.8 ± 0.7	0.815 ± 0.009	0	-1	0
oΛCDM	0.309 ± 0.011	67.6 ± 1.1	0.813 ± 0.011	-0.001 ± 0.003	-1	0
wCDM	0.311 ± 0.022	67.6 ± 2.4	0.813 ± 0.023	0	-0.99 ± 0.09	0
owCDM	0.308 ± 0.023	67.8 ± 2.5	0.815 ± 0.024	-0.001 ± 0.004	-1.01 ± 0.11	0
w_0w_aCDM	0.329 ± 0.033	65.9 ± 3.4	0.798 ± 0.030	0	-0.78 ± 0.29	-0.60 ± 0.74
ow_0w_aCDM	0.330 ± 0.033	65.6 ± 3.4	0.799 ± 0.029	-0.003 ± 0.004	-0.75 ± 0.28	-0.81 ± 0.77
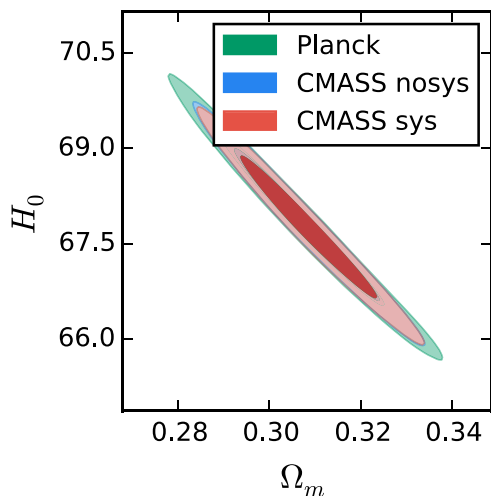
Figure 2. 2D marginalized contours for 68 per cent and 95 per cent confidence levels for Ω_m and H_0 (ΛCDM model assumed) from *Planck*-only (green), *Planck*+CMASS (red), and *Planck*+CMASS without including systematics weights (blue).

Figure 3. 2D marginalized contours for 68 per cent and 95 per cent confidence level for Ω_m and Ω_k (oΛCDM model assumed) from *Planck*-only (green), *Planck*+CMASS (red), and *Planck*+CMASS without including systematics weights (blue). One can see that Ω_k is consistent with 0 which is corresponding to the flat universe.

contours comparing with *Planck* CMB data (Planck Collaboration I 2015) in Figs 2–7. One can see that the constraints obtained from our measurements without including observational systematics weights agree very well with the corrected ones. In addition, we do not find any deviation from ΛCDM by testing various models.

6 COMPARISON WITH OTHER WORKS

The constraints on $H(z)r_s/r_{s,\mathrm{fid}}$ and $D_A(z)r_{s,\mathrm{fid}}/r_s$ are dominated by the two-dimensional BAO feature. As shown in fig. 13 of Anderson et al. (2014a), the measurements were similar between the results from the analyses with (green) and without (blue and red) the full shape information. Note, in the same plot, the constraints from Reid et al. (2012) (purple) and Sanchez et al. (2013a) (black) were tighter because they either included much smaller scales or used stronger dark energy model assumption. The recent BAO-only measurements are replying on the BAO reconstruction methodologies, e.g.

see Anderson et al. (2014b); Cuesta et al. (2016); Gil-Marin et al. (2015a). In those analyses, the BAO feature was enhanced but the full shape information was removed. Therefore, the information obtained from the BAO-only measurements is different from ours. BAO-only analyses do not provide $f(z)\sigma_8(z)$ measurements which could be useful for testing gravity theory, e.g. see Samushia et al. (2013, 2014); Beutler et al. (2014); Alam et al. (2015). Gil-Marin et al. (2015b) extracted the cosmological information from the full shape information using similar data sample as ours, but they performed the analysis in the Fourier space. The systematics considered in our studies have only impact on the small k-mode that they do not use. However, the non-linear evolution and non-linear redshift space distortion at small scales in configuration space would propagate to larger range of k-mode in Fourier space.
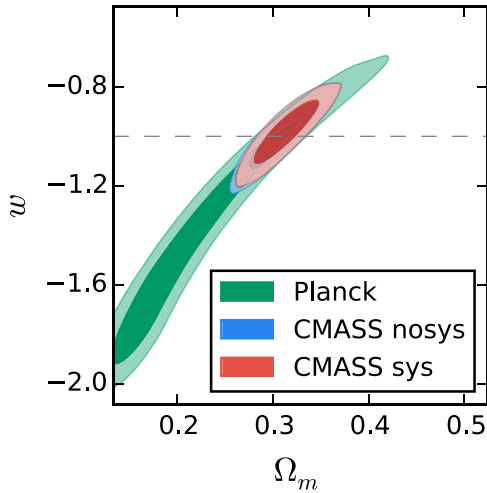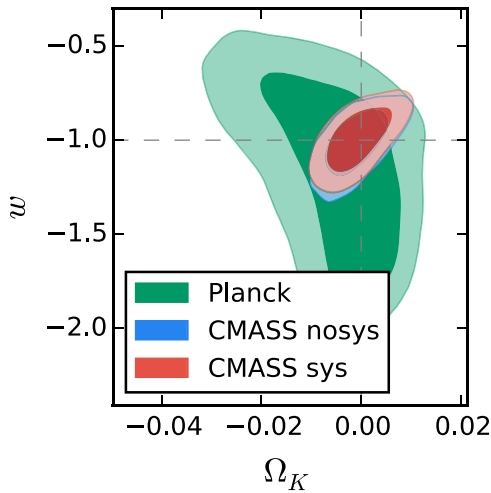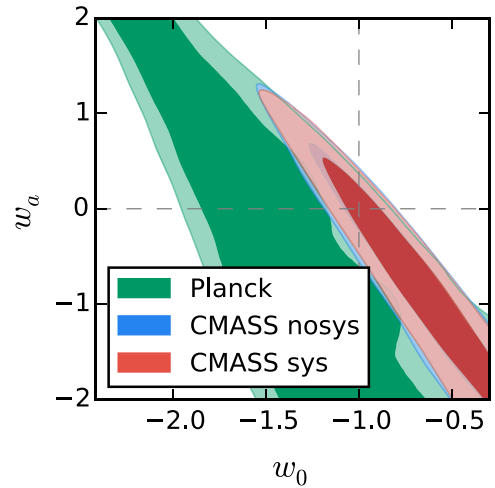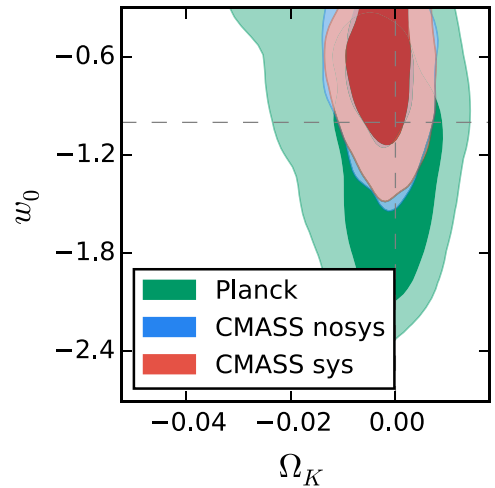
Figure 4. 2D marginalized contours for 68 per cent and 95 per cent confidence level for Ω_m and w (wCDM model assumed) from *Planck*-only (green), *Planck*+CMASS (red), and *Planck*+CMASS without including systematics weights (blue). One can see that w is consistent with -1 which is corresponding to the ΛCDM.

Figure 6. 2D marginalized contours for 68 per cent and 95 per cent confidence level for w_0 and w_a (w_0w_aCDM model assumed) from *Planck*-only (green), *Planck*+CMASS (red), and *Planck*+CMASS without including systematics weights (blue). One can see that w_0 and w_a are consistent with -1 and 0, respectively which are corresponding to the ΛCDM.

Figure 5. 2D marginalized contours for 68 per cent and 95 per cent confidence level for Ω_k and w (wCDM model assumed) from *Planck*-only (green), *Planck*+CMASS (red), and *Planck*+CMASS without including systematics weights (blue). One can see that Ω_k is consistent with 0 and w is consistent with -1 which is corresponding to the ΛCDM.

Figure 7. 2D marginalized contours for 68 per cent and 95 per cent confidence level for Ω_k and w_0 (ow_0w_aCDM model assumed) from *Planck*-only (green), *Planck*+CMASS (red), and *Planck*+CMASS without including systematics weights (blue). One can see that Ω_k and w_0 are consistent with 0 and -1, respectively which are corresponding to the ΛCDM.

The redshift range used in our analysis for DR12 CMASS (0.43 $< z <$ 0.75) is slightly different from the range used by Gil-Marin et al. (2015b) (0.43 $< z <$ 0.7). We intend to use larger volume of the sample to increase the statistics power since we drop smaller scales ($s <$ 55 Mpc) to minimize scale-dependent effects and measure unbiased growth rate as mentioned. If we rescale our measurements to the same effective redshift $z =$ 0.57 of Gil-Marin et al. (2015b), we obtain $H(0.57)r_s =$ (14.29 $\pm$ 0.48) $\times 10^3$ km s^{-1}, $DA(0.57)/r_s$ = 9.44 $\pm$ 0.17 and $f(z_{eff})\sigma_8(z_{eff})$ = 0.488 $\pm$ 0.060 ($f\sigma_8$ is insensitive to the effective redshift). Despite of the different redshift range and methodology used, our measurements are in good agreement with the results from Gil-Marin et al. (2015b), $H(0.57)r_s =$ (13.92 $\pm$

0.44) $\times 10^3$ km/s, $D_A(0.57)/r_s =$ 9.42 $\pm$ 0.15, and $f(z_{eff})\sigma_8(z_{eff})$ = 0.444 $\pm$ 0.038.

In Figs 8–11, we compare the constraints of $f(z)\sigma_8(z)$, $D_A(z)/r_s$, $H(z)r_s$, and $D_V(z)/r_s$ from CMB data (*Planck* assuming LCDM) with the measurements from galaxy clustering analyses. We have included the measurements from VIMOS-VLT Deep Survey (VVDS; Guzzo et al. 2008), 2dFGRS (Percival et al. 2004), Six-degree-Field Galaxy Survey (6dFGS; Beutler et al. 2012), WiggleZ (Blake et al. 2011a,b), SDSS-II/DR7 (Percival et al. 2010; Samushia et al. 2011; Chuang & Wang 2012, 2013a,b; Chuang et al. 2012; Padmanabhan et al. 2012; Seo et al. 2012; Xu et al. 2013; Hemantha et al. 2014; Ross et al. 2015) SDSS-III/BOSS (Reid et al. 2012, 2014; Anderson et al. 2013, 2014a,b; Chuang et al. 2013; Kazin et al. 2013;
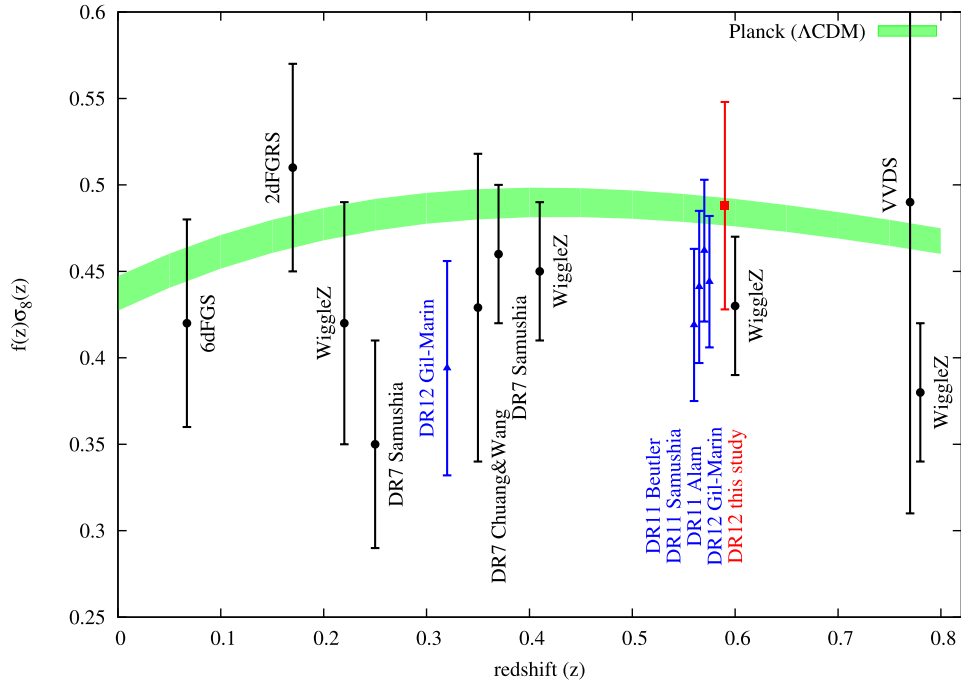
Figure 8. We compare the constraints of $f(z)\sigma_8(z)$ from CMB data (*Planck*) with our measurement (red square), other measurements from BOSS galaxy sample (blue triangle; Beutler et al. 2014; Samushia et al. 2014; Alam et al. 2015; Gil-Marin et al. 2015a) and the measurements compiled by Samushia et al. (2013) (black circles). The constraints from CMB are obtained given ΛCDM model.
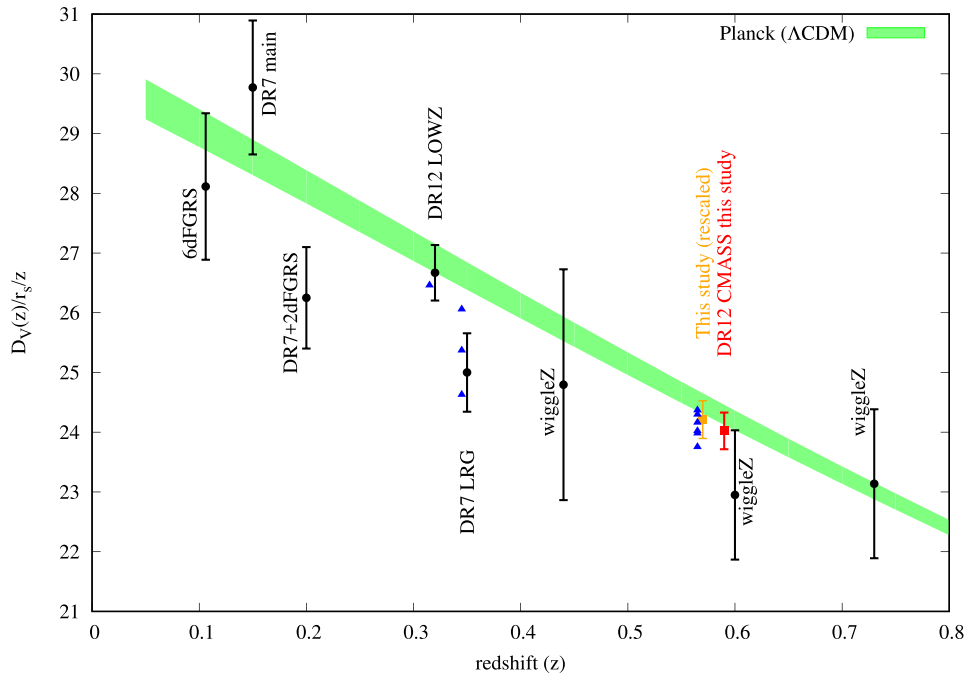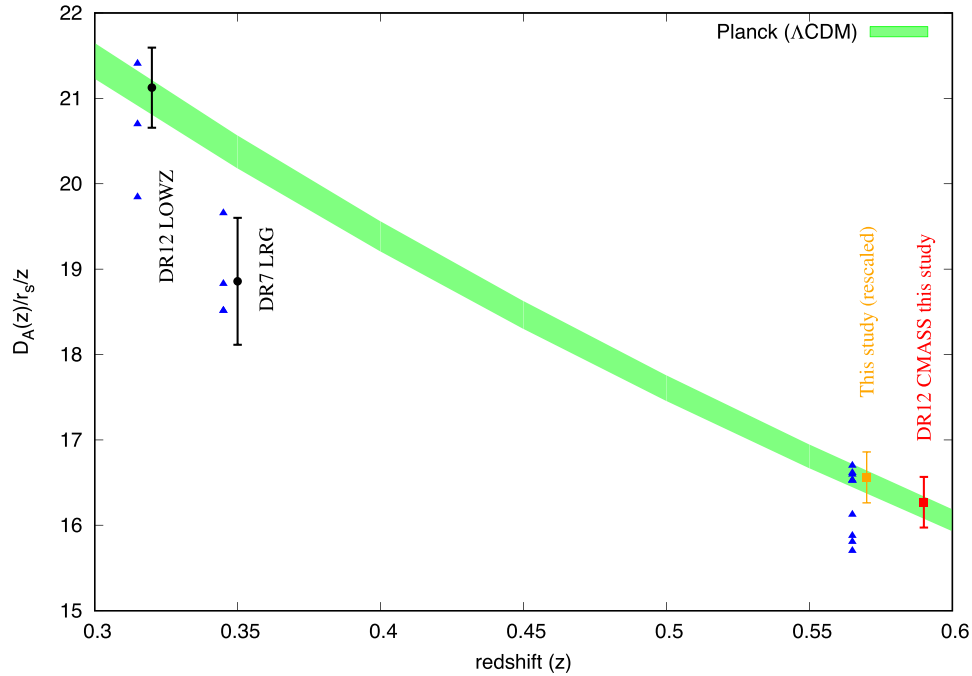

Figure 9. We compare the constraints of $\frac{D_V(z)}{r_s z}$ from CMB data (*Planck*) with our measurement (red square), and other measurements (black circles and blue triangles; Percival et al. 2010; Blake et al. 2011a; Beutler et al. 2012, 2014; Chuang & Wang 2012; Chuang et al. 2012; Padmanabhan et al. 2012; Anderson et al. 2013, 2014b; Samushia et al. 2014; Tojeiro et al. 2014; Ross et al. 2015). When there are more than one measurements at the same redshift, we mark one of the measurement using a black circle with error bar (i.e. the measurement from Chuang & Wang 2012 at $z = 0.35$ and the measurement from Cuesta et al. 2016 at $z = 0.32$) and mark the others with blue triangles with slight shift in redshift to make the plot more clear. The constraints from CMB are obtained given ΛCDM model.
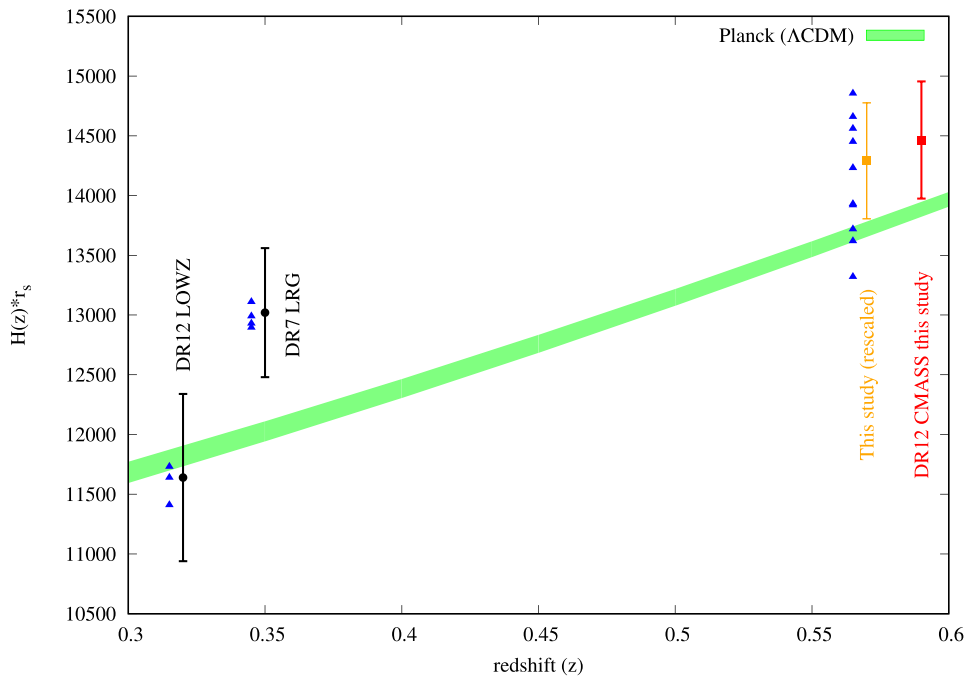
Figure 10. We compare the constraints of $\frac{D_A(z)}{r_s z}$ from CMB data (*Planck*) with our measurement (red square), and other measurements (black circles and blue triangles; Chuang & Wang 2012, 2013a,b; Chuang et al. 2013; Kazin et al. 2013; Xu et al. 2013; Anderson et al. 2014a,b; Beutler et al. 2014; Hemantha et al. 2014; Wang 2014; Gil-Marin et al. 2015a,b; Cuesta et al. 2016). When there are more than one measurements at the same redshift, we mark one of the measurement using a black circle with error bar (i.e. the measurement from Chuang & Wang 2012 at $z = 0.35$ and the consensus value from Gil-Marin et al. 2015a; Cuesta et al. 2016 at $z = 0.32$) and mark the others with blue triangles with slight shift in redshift to make the plot more clear. The constraints from CMB are obtained given ΛCDM model.

Figure 11. We compare the constraints of $H(z)r_s$ from CMB data (*Planck*) with our measurement (red square), and other measurements (black circles and blue triangles; Chuang & Wang 2012, 2013a,b; Chuang et al. 2013; Kazin et al. 2013; Xu et al. 2013; Anderson et al. 2014a,b; Beutler et al. 2014; Hemantha et al. 2014; Wang 2014; Gil-Marin et al. 2015a,b; Cuesta et al. 2016). When there are more than one measurements at the same redshift, we mark one of the measurement using a black circle with error bar (i.e. the measurement from Chuang & Wang 2012 at $z = 0.35$ and the consensus value from Gil-Marin et al. 2015a; Cuesta et al. 2016 at $z = 0.32$) and mark the others with blue triangles with slight shift in redshift to make the plot more clear. The constraints from CMB are obtained given ΛCDM model.

Sanchez et al. 2013a; Beutler et al. 2014; Samushia et al. 2014; Tojeiro et al. 2014; Wang 2014; Alam et al. 2015; Gil-Marin et al. 2015a,b; Cuesta et al. 2016)

In Figs 9–11, when there are multiple measurements that are corresponding the same redshifts, we show the mean and error bar for one of them (indicated in the captions) and show only the means with triangles for the rest of the measurements. We also slightly shift the redshift to make the figures more clear. One can see that the measurements of $D_V(z)r_{s,\mathrm{fid}}/r_s$ and $f(z)\sigma_8(z)$ from different analyses but at the same redshift agree with each other. However, the measurements of $H(z)r_s/r_{s,\mathrm{fid}}$ and $D_A(z)r_{s,\mathrm{fid}}/r_s$ have larger scatter. This is expected since $D_V(z)r_{s,\mathrm{fid}}/r_s$ measurement is driven by the BAO feature in the monopole and $f(z)\sigma_8(z)$ is mainly determined by the amplitude of quadrupole. But, $H(z)r_s/r_{s,\mathrm{fid}}$ and $D_A(z)r_{s,\mathrm{fid}}/r_s$ is correlated with the shape of BAO feature which has larger uncertainties among different models. In addition, we rescale our measurements of $H(z)r_s/r_{s,\mathrm{fid}}$, $D_A(z)r_{s,\mathrm{fid}}/r_s$, and $D_V(z)r_{s,\mathrm{fid}}/r_s$, from the effective redshift $z = 0.59$ (the points with red solid error bars) to $z = 0.57$ (the orange points with thiner error bars) for the convenience of comparison with previous works. One can see our measurements are in agreement with others.

7 SUMMARY

We present measurements of the anisotropic galaxy clustering from the DR12 CMASS samples of the SDSS-III Baryon Oscillation Spectroscopic Survey (BOSS). We analyse the broad-range shape of quasi-linear scales, which can be modelled by perturbation theory, of the monopole and quadrupole correlation functions to obtain cosmological constraints, at the effective redshift $z = 0.59$ of the sample, on the Hubble expansion rate $H(z)$, the angular diameter distance $D_A(z)$, the normalized growth rate $f(z)\sigma_8(z)$, and the physical matter density $\Omega_m h^2$. We obtain more robust measurements by including a polynomial as the model for the systematic errors. We find it works very well against the systematics effects, e.g. effects from stars and seeing. The parameters which are not well constrained by our galaxy clustering analysis are marginalized over with wide flat priors. Since no priors from other data sets (i.e. CMB) are adopted and no dark energy models are assumed, our results from BOSS CMASS galaxy clustering may be combined with other data sets, i.e. CMB, SNe, lensing or other galaxy clustering data to constrain the parameters of a given cosmological model. Our main results can be summarized as follows.

(i) Our measurements for DR12 CMASS ($0.43 < z < 0.75$), using the range $55\,h^{-1}$ Mpc $< s < 200\,h^{-1}$ Mpc, are $\{D_A(0.59)r_{s,\mathrm{fid}}/r_s,$ $H(0.59)r_s/r_{s,\mathrm{fid}}, f(0.59)\sigma_8(0.59), \Omega_m h^2\} = \{1427 \pm 26, 97.3 \pm 3.3,$ $0.488 \pm 0.060, 0.135 \pm 0.016\}$, where r_s is the comoving sound horizon at the drag epoch and $r_{s,\mathrm{fid}}$ is the r_s of the fiducial cosmology used in this study.

(ii) In the case of the cosmological model assuming ΛCDM, our single-probe constraints from CMASS quasi-linear scales, combined with CMB (*Planck*), yield the values for $\Omega_m = 0.308 \pm 0.010$ and $H_0 = 67.8 \pm 0.7$ kms^{-1} Mpc^{-1}; considering oΛCDM (non-flat ΛCDM), we obtain the curvature density fraction, $\Omega_k = -0.001 \pm 0.003$; adopting a constant dark energy equation of state and a flat universe (wCDM), the constraint on dark energy equation-of-state parameter is $w = -0.98 \pm 0.08$.

(iii) Using our methodology and the correlation function measured without including the systematics weights corrections, we obtain the same results as the ones including the systematics weights corrections. We conclude that our measurements are robust against the known observational systematics.

REFERENCES

Abazajian K. et al. (SDSS Collaboration), 2005, AJ, 129, 1755
Abazajian K. N. et al. (SDSS Collaboration), 2009, ApJS, 182, 543
Alam S. et al. (SDSS-III Collaboration), 2015, ApJS, 219, 12
Alam S., Ho S., Vargas-Magaña M., Schneider D. P., 2015, MNRAS, 453, 1754
Alcock C., Paczynski B., 1979, Nature, 281, 358
Anderson L. et al., 2013, MNRAS, 428, 1036
Anderson L. et al., 2014a, MNRAS, 439, 83
Anderson L. et al. (BOSS Collaboration), 2014b, MNRAS, 441, 24
Beutler F. et al., 2012, MNRAS, 423, 3430
Beutler F. et al. (BOSS Collaboration), 2014, MNRAS, 443, 1065
Blake C., Collister A., Bridle S., Lahav O., 2007, MNRAS, 374, 1527
Blake C. et al., 2011a, MNRAS, 418, 1707
Blake C. et al., 2011b, MNRAS, 418, 1725
Blake C. et al., 2012, MNRAS, 425, 405
Bolton A. S. et al., 2012, AJ, 144, 144
Cabre A., Gaztanaga E., 2009, MNRAS, 393, 1183
Chuang C. H. et al., 2015, MNRAS, 452, 686
Chuang C.-H. et al., 2016, preprint (arXiv:1607.03151)
Chuang C.-H., Wang Y., 2012, MNRAS, 426, 226
Chuang C.-H., Wang Y., 2013a, MNRAS, 431, 2634
Chuang C.-H., Wang Y., 2013b, MNRAS, 435, 255
Chuang C.-H., Wang Y., Hemantha M. D. P., 2012, MNRAS, 423, 1474

Chuang C.-H. et al., 2013, MNRAS, 433, 3559
Colless M. et al. (The 2DFGRS Collaboration), 2001, MNRAS, 328, 1039
Colless M. et al., 2003, preprint (astro-ph/0306581)
Crocce M., Scoccimarro R., 2006, Phys. Rev. D, 73, 063520
Cuesta A. J. et al., 2016, MNRAS, 457, 1770
Dawson K. S. et al. (BOSS Collaboration), 2013, AJ, 145, 10
Drinkwater M. J. et al., 2010, MNRAS, 401, 1429
Eisenstein D. J. et al. (SDSS Collaboration), 2001, AJ, 122, 2267
Eisenstein D. J. et al. (SDSS Collaboration), 2005, ApJ, 633, 560
Eisenstein D. J., Hu W., 1998, ApJ, 496, 605
Eisenstein D. J., Seo H.-J., White M. J., 2007, ApJ, 664, 660
Eisenstein D. J. et al., 2011, AJ, 142, 72
Feldman H. A., Kaiser N., Peacock J. A., 1994, ApJ, 426, 23
Fukugita M., Ichikawa T., Gunn J. E., Doi M., Shimasaku K., Schneider
    D. P., 1996, AJ, 111, 1748
Gil-Marín H. et al., 2015a, MNRAS, preprint (arXiv:1509.06373)
Gil-Marín H. et al., 2015b, MNRAS, preprint (arXiv:1509.06386)
Green J. et al., 2012, preprint (arXiv:1208.4012)
Gunn J. E. et al. (SDSS Collaboration), 1998, AJ, 116, 3040
Gunn J. E. et al. (SDSS Collaboration), 2006, AJ, 131, 2332
Guzzo L. et al., 2008, Nature, 451, 541
Hartlap J., Simon P., Schneider P., 2007, A&A, 464, 399
Hemantha M. D. P., Wang Y., Chuang C. H., 2014, MNRAS, 445, 3737
Hinshaw G. et al., 2013, ApJS, 208, 19
Hutsi G., 2005, preprint (astro-ph/0507678)
Kaiser N., 1987, MNRAS, 227, 1
Kazin E. A. et al., 2010, ApJ, 710, 1444
Kazin E. A. et al., 2013, MNRAS, 435, 64
Kitaura F. S., Hess S., 2013, MNRAS, 435, 78
Kitaura F. S., Yepes G., Prada F., 2014, MNRAS, 439, 21
Kitaura F. S., Gil-Marín H., Scoccola C., Chuang C. H., Müller V., Yepes
    G., Prada F., 2015, MNRAS, 450, 1836
Kitaura F. S. et al., 2016, MNRAS, 456, 4156
Klypin A., Yepes G., Gottlober S., Prada F., Hess S., 2016, MNRAS, 457,
    4340
Landy S. D., Szalay A. S., 1993, ApJ, 412, 64
Laureijs R. et al., 2011, preprint (arXiv:1110.3193)
Lewis A., Bridle S., 2002, Phys. Rev. D 66, 103511
Lewis A., Challinor A., Lasenby A., 2000, ApJ, 538, 473
Manera M. et al., 2013, MNRAS, 428, 1036
Manera M. et al., 2015, MNRAS, 447, 437
Martinez V. J. et al., 2009, ApJ, 696, L93 (Erratum-ibid., 2009, ApJ, 703,
    L184)
Matsubara T., 2008, Phys. Rev. D, 77, 063530
Montesano F., Sanchez A. G., Phleps S., 2012, MNRAS, 421, 2656
Nuza S. E. et al., 2013, MNRAS, 432, 743
Oka A., Saito S., Nishimichi T., Taruya A., Yamamoto K., 2014, MNRAS,
    439, 2515
Okumura T., Matsubara T., Eisenstein D. J., Kayo I., Hikage C., Szalay
    A. S., Schneider D. P., 2008, ApJ, 676, 889
Padmanabhan N., et al ., (SDSS Collaboration), 2007, MNRAS, 378, 852
Padmanabhan N., Xu X., Eisenstein D. J., Scalzo R., Cuesta A. J., Mehta
    K. T., Kazin E., 2012, MNRAS, 427, 2132
Parkinson D. et al., 2012, Phys. Rev. D, 86, 103518
Percival W. J., White M., 2009, MNRAS, 393, 297
Percival W. J. et al. (2dFGRS Collaboration), 2004, MNRAS, 353, 1201
Percival W. J., Cole S., Eisenstein D. J., Nichol R. C., Peacock J. A., Pope
    A. C., Szalay A. S., 2007, MNRAS, 381, 1053
Percival W. J. et al., 2010, MNRAS, 401, 2148
Perlmutter S. et al. (Supernova Cosmology Project Collaboration), 1999,
    ApJ, 517, 565
Planck Collaboration I 2014a, A&A, 571, A1
Planck Collaboration XVI 2014b, A&A, 571, A16
Planck Collaboration I 2015, preprint (arXiv:1502.01582)
Press W. H., Teukolsky S, A. Vetterling W. T., Flannery B. P., 1992, Numer-
    ical Recipes in C. The Art of Scientific Computing, 2nd edn. Cambridge
    Univ. Press, Cambridge
Reid B. A. et al., 2010, MNRAS, 404, 60
Reid B. A. et al., 2012, MNRAS, 426, 2719
Reid B. A., Seo H. J., Leauthaud A., Tinker J. L., White M., 2014, MNRAS,
    444, 476
Reid B. et al., 2016, MNRAS, 455, 1553
Riess A. G. et al. (Supernova Search Team Collaboration), 1998, AJ, 116,
    1009
Rodríguez-Torres S. A. et al., 2016, MNRAS, 460, 1173
Ross A. J. et al. (BOSS Collaboration), 2012, MNRAS, 424, 564
Ross A. J., Samushia L., Howlett C., Percival W. J., Burden A., Manera M.,
    2015, MNRAS, 449, 835
Samushia L., Percival W. J., Raccanelli A., 2011, MNRAS, 420, 2102
Samushia L. et al., 2013, MNRAS, 429, 1514
Samushia L. et al., 2014, MNRAS, 439, 3504
Sanchez A. G., Crocce M., Cabre A., Baugh C. M., Gaztanaga E., 2009,
    MNRAS, 400, 1643
Sanchez A. G. et al., 2013a, MNRAS, 433, 1202
Schlegel D. et al. (BigBoss Experiment Collaboration), 2011, preprint
    (arXiv:1106.1706)
Seo H. et al., 2012, ApJ, 761, 1, 13
Smee S. et al., 2013, AJ, 146, 32
Song Y.-S., Percival W. J., 2009, J. Cosmol. Astropart. Phys., 10, 004
Tegmark M. et al. (SDSS Collaboration), 2004, ApJ, 606, 702
Tojeiro R. et al., 2012, MNRAS, 424, 2339
Tojeiro R. et al., 2014, MNRAS, 440, 2222
Van Waerbeke L., Mellier Y., 2003, preprint (astro-ph/0305089)
Verde L. et al., 2001, preprint (astro-ph/0112161]
Wang Y., 2008, J. Cosmol. Astropart. Phys., 05, 021
Wang Y., 2012, MNRAS, 423, 3631
Wang Y., 2014, MNRAS, 443, 2950
Xu X., Cuesta A. J., Padmanabhan N., Eisenstein D. J., McBride C. K.,
    2013, MNRAS, 431, 2834
York D. G. et al. (SDSS Collaboration), 2000, AJ, 120, 1579

[1]*Instituto de Física Teórica, (UAM/CSIC), Universidad Autónoma de Madrid, Cantoblanco, E-28049 Madrid, Spain*
[2]*Leibniz-Institut für Astrophysik Potsdam (AIP), An der Sternwarte 16, D-14482 Potsdam, Germany*
[3]*Campus of International Excellence UAM+CSIC, Cantoblanco, E-28049 Madrid, Spain*
[4]*Instituto de Astrofísica de Andalucía (CSIC), Glorieta de la Astronomía, E-18080 Granada, Spain*
[5]*Instituto de Astrofísica de Canarias (IAC), C/Vía Láctea, s/n, E-38200 La Laguna, Tenerife, Spain*
[6]*Departamento Astrofísica, Universidad de La Laguna (ULL), E-38206 La Laguna, Tenerife, Spain*
[7]*Lawrence Berkeley National Lab, 1 Cyclotron Rd, Berkeley, CA 94720, USA*
[8]*Institute of Cosmology and Gravitation, University of Portsmouth, Dennis Sciama Building, Portsmouth PO1 3FX, UK*
[9]*Institut de Ciències del Cosmos (ICCUB), Universitat de Barcelona (IEEC-UB), Martí i Franquès 1, E-08028 Barcelona, Spain*
[10]*Harvard–Smithsonian Center for Astrophysics, 60 Garden St, Cambridge, MA 02138, USA*
[11]*CPPM, Aix-Marseille Université, CNRS/IN2P3, F-13288 Marseille, France*
[12]*Department of Physics, Carnegie Mellon University, 5000 Forbes Ave., Pittsburgh, PA 15213, USA*
[13]*Departments of Physics and Astronomy, University of California, Berkeley, CA 94720, USA*
[14]*Laboratoire d'astrophysique, École Polytechnique Fédérale de Lausanne (EPFL), Observatoire de Sauverny, CH-1290 Versoix, Switzerland*
[15]*Aix Marseille Université, CNRS, LAM (Laboratoire d'Astrophysique de Marseille) UMR 7326, F-13388 Marseille, France*
[16]*Department of Physics and Astronomy, University College London, Gower Street, London WC1E 6BT, UK*
[17]*Departamento de Física Teórica M8, Universidad Autonoma de Madrid (UAM), Cantoblanco, E-28049 Madrid, Spain*

[18] *Center for Cosmology and Astroparticle Physics, Department of Physics, The Ohio State University, OH 43210, USA*

[19] *Kansas State University, Manhattan, KS 66506, USA*

[20] *National Abastumani Astrophysical Observatory, Ilia State University, 2A Kazbegi Ave., GE-1060 Tbilisi, Georgia*

[21] *Department of Astronomy and Astrophysics, The Pennsylvania State University, University Park, PA 16802, USA*

[22] *Institute for Gravitation and the Cosmos, The Pennsylvania State University, University Park, PA 16802, USA*

[23] *National Astronomy Observatories, Chinese Academy of Science, Beijing 100012, P.R.China*

[24] *Center for Cosmology and Particle Physics, New York University, New York, NY 10003, USA*

[25] *Department of Physics and Astronomy, University of Utah, 115 S 1400 E, Salt Lake City, UT 84112, USA*

[26] *Department of Chemistry and Physics, King's College, 133 North River St, Wilkes Barre, PA 18711, USA*

This paper has been typeset from a TEX/LATEX file prepared by the author.